Journal of Colloid and Interface Science 541 (2019) 312–321

Contents lists available at ScienceDirect

Journal of Colloid and Interface Science

journal homepage: www.elsevier.com/locate/jcis

Regular Article

Dynamics of stain growth from sessile droplets on paper

Michael J. Hertaeg [a], Rico F. Tabor [b], Joseph D. Berry [c], Gil Garnier [a,*]

[a] BioPRIA and Department of Chemical Engineering, Monash University, Clayton, VIC 3800, Australia
[b] School of Chemistry, Monash University, Clayton, VIC 3800, Australia
[c] Department of Chemical and Biomolecular Engineering and the Particulate Fluids Processing Centre, University of Melbourne, Parkville, Victoria 3010, Australia

GRAPHICAL ABSTRACT

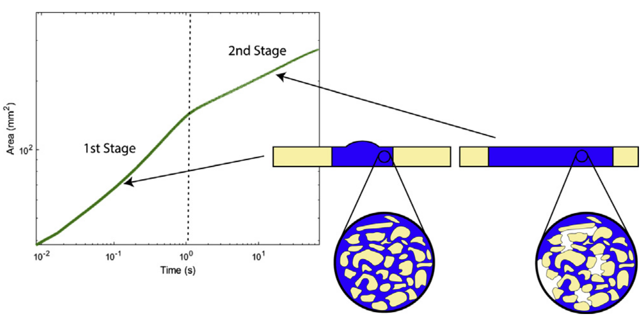

ARTICLE INFO

Article history:
Received 29 November 2018
Revised 8 January 2019
Accepted 9 January 2019
Available online 16 January 2019

Keywords:
Radial wicking
Stain area
Paper
Wetting
Kinetics
Modelling
Sessile droplets

ABSTRACT

Hypothesis: The rate of stain growth of a sessile droplet deposited on paper has been previously studied (Kissa, 1981; Danino and Marmur, 1994; Kawase et al., 1986; Borhan and Rungta, 1993) but is not fully understood. In particular, the mechanism by which the abrupt decrease in growth rate occurs is unknown. This process is expected to follow a model where the disappearance of the droplet is represented by a change to the boundary condition at the droplet-paper interface when the volume of the fluid inside the paper is equal to the volume of the simulated droplet.

Experiments: The stain size of sessile droplets on paper was monitored against time. A series of fluids varying in surface tension and viscosity was studied. The kinetics of stain growth was modelled and compared with experiments and existing models of stain growth.

Findings: The measured stain area formed by a sessile droplet deposited on paper follows a two regime mechanism (Danino and Marmur, 1994). In the initial regime, the dynamics are governed by the filling of pores. However, in the later stage, the process is influenced by the emptying/redistribution of fluid. Simulations show that experimental results are well described by a model that identifies the change in boundary conditions after the droplet is no longer present above the paper, coupled with the change to a redistribution dominated mechanism.

1. Introduction

Wicking has been described for many years by the Lucas-Washburn equation [5,6]. This model assumes the substrate material to be a collection of cylindrical capillaries and gives fairly good correlation with experimental results in a variety of porous materials [7,8]. However, there are several critical and restrictive simplifications required that prevent generalisation of the model to all wicking applications. The two most notable assumptions of the Lucas-Washburn equation are: (i) the unidirectional requirements and (ii) the definition of a sharp interface where the

* Corresponding author.
E-mail address: Gil.Garnier@monash.edu (G. Garnier).

https://doi.org/10.1016/j.jcis.2019.01.032

material transitions from 100% saturated to 0% saturated at the wicking front. These two assumptions do not apply for many systems including droplets wicking on paper. To overcome these simplifications, previous researchers have derived relations based on Darcy's law for flow through porous media. These approaches allow for the description of wicking in complex geometries and semi-saturated media and are used in the design of many paper-based diagnostic devices [9].

The deposition of a droplet of liquid onto the surface of a thin porous material like paper is a special wicking case that has received particular attention. Droplets wicking on porous media and the kinetics of stain growth play a critical role in many industrial applications, including printing for communication and functional uses such as biodiagnostic manufacturing. Fundamentally, modelling the kinetics of droplet wicking, from sessile droplet to stain at equilibrium, has remained a complex and elusive task. This process is different from the case of a infinite reservoir system because at some finite time after deposition, the droplet will completely be absorbed by the paper, changing the nature of the process significantly. These two stages are usually referred to as stage one (droplet disappearing from the surface of the paper) and stage two (absorbed droplet redistributing/wicking in paper). As stage two is much longer than stage one, most of the models have been focused there. Many models based on Darcy's law have been proposed. However, all have relied on many empiricisms to fit results [1,2,10,11]. All of these relations can be broadly expressed in the functional form:

$$A \propto t^m, \tag{1}$$

where A is the wetted area, t the time after deposition and m is a constant. The evolution of the stain area produced by a wicking droplet is quite well represented by this power law. However, the value of m is higher in the first stage than in the second stage. The stated values of m for each stage vary but are in the range of 0.39–0.50 for the first stage and 0.10–0.33 for the second stage [1–4]. These discrepancies have been attributed to differences between fluids, droplet sizes, absorption by fibers, temperature and humidity; however, no model has been able to explain the large variation reported.

Marmur [12] presented an analytical model for radial wicking where the material is modelled as a gap between two plates with liquid being introduced from a hole in the center of the top plate. Marmur's equation expressed in terms of area [4] is given as:

$$\frac{A}{A_o}\left(\ln\frac{A}{A_o} - 1\right) = -1 + \left(\frac{2\pi d\gamma\cos\theta}{3A_o\mu}\right)t. \tag{2}$$

Here A is wetted area, A_o is the area of the inlet, d is the separation of the two plates, γ is the liquid–vapour surface tension of the liquid, θ is the contact angle and μ is the viscosity. This approach is similar to that of Lucas and Washburn as it also assumes a sharp interface. Despite this, the equation predicts radial wicking behavior from infinite reservoirs quite well [2,4] and results from Danino and Marmur [2] imply that it also can be used to model stage one of droplet wicking. For the droplet wicking case, it is not clear what value to use for A_o; however, the fitted values are physically reasonable.

The effectiveness of Marmur's equation in predicting stage one behavior implies that the distribution of fluid creates an abrupt transition between fully saturated and dry paper. However, after the consumption of the reservoir (stage two), liquid motion is primarily driven by the redistribution effect [13] which is why Marmur's equation is no longer appropriate. The redistribution effect is the emptying of initially filled large pores into smaller pores due to the higher capillary pressures there. Our previous work has identified that this motion will continue until a position is reached that is determined by the system's solid–liquid interfacial energy [14].

Several numerical studies have predicted wicking behavior from infinite reservoirs using Richards' equation, developed to determine liquid distribution in soils [15–18]. Some of these studies simulate radial wicking and correlate well with both experimental results and Marmur's relation (Eq. (2)). The present work applies previously developed numerical schemes to model the radial wicking of fluid from a sessile droplet. This is done by applying the same Dirichlet (saturated) boundary conditions [19] used for infinite systems at the droplet interface until the simulated droplet is consumed. After this a Neumann (no flux) boundary condition [19] is used.

It is the objective of this study to measure and model the wicking dynamics of a sessile droplet deposited onto paper. We also aim to identify and quantify the mechanisms controlling the stain growth in paper. This knowledge is required to engineer accurate and predictive paper diagnostics for biomedical applications [20]. A secondary objective of the study is to develop a rigorous, accurate and physically meaningful alternative to the Lucas-Washburn equation.

2. Methods

2.1. Simulation

2.1.1. Model development

Richards' equation can be described as Darcy's law with allowances for mass conservation where the permeability of the porous material is proportional to the local volume fraction [21],

$$\frac{\partial\phi}{\partial t} = \nabla\cdot\left(\frac{K(\phi)}{\mu}\nabla P\right) \tag{3}$$

here ϕ is the relative volume fraction expressed relative to maximum saturation $\phi = \epsilon/\epsilon_s$, ϵ is the volume fraction expressed in volume of fluid per volume of paper and ϵ_s is the saturated volume fraction, $K(\phi)$ is the permeability as a function of volume fraction, μ is viscosity and P is pressure.

In a wicking situation where there is no externally applied pressure gradient and gravitational effects can be ignored, pressure variation is caused solely by Laplace pressure at liquid–vapour interfaces. This pressure will be a function of volume fraction as the liquid–vapour interfaces will be in small pores with higher Laplace pressures at low volume fractions, and will move to large pores with lower Laplace pressures at high volume fractions. With this, Eq. (3) becomes the diffusion equation where diffusivity is a simple function of pressure, permeability and viscosity:

$$\frac{\partial\phi}{\partial t} = \nabla\cdot\left(\frac{D(\phi)}{\mu}\nabla\phi\right), \tag{4}$$

$$D(\phi) = K(\phi)\frac{\partial P(\phi)}{\partial\phi}. \tag{5}$$

This approach was verified by several previous studies [15–18]. However, each of those used a different function for permeability and pressure distribution. One of the simplest systems of constitutive equations for permeability and pressure was implemented by Perez-Cruz [15] and is reproduced here. This model expresses the combined effects of varying pressure and permeability as an effective scaled diffusivity. Due to the factor of viscosity in Eq. (4), $D(\phi)$ is not a true diffusivity and therefore does not have the units m^2/s. This scaled diffusivity can be expressed as a power law relation with volume fraction [15]:

$$D(\phi) = D_0\phi^n \tag{6}$$

where D_0 is the viscosity scaled diffusivity at saturation and n is a constant calculated from a substrate's pore size distribution index [22]. Perez-Cruz fit n to results. However, pore size distribution index (λ), and therefore n, can be calculated by fitting Eq. (7) to experimental porosimetry data (Fig. 3):

$$\phi = \left(\frac{P(\phi)}{P_c}\right)^{-\lambda}, \tag{7}$$

$$n = 2 + \frac{1}{\lambda}, \tag{8}$$

where P_c is atmospheric pressure. These relations are based on the Brooks Corey model for water penetration in soils [22].

2.1.2. Model implementation

The solution of Eq. (4) was carried out in arb, an open source finite volume solver [23] on a two-dimensional axisymmetric domain (Fig. 1). Boundary conditions were initially no flux on all external edges, except the top region covered by the droplet at $0 > r > R_0$. Here, the value of phi was fixed at the saturation value of the material until the total volume of liquid in the domain reaches the volume of the simulated droplet at $t = t_{abs}$. For $t > t_{abs}$ the boundary condition at the droplet interface was changed to the zero flux condition. This procedure simulates the transition from stage one to stage two radial wicking where the droplet disappears from the surface of the paper. This process ignores the changes in droplet radius discussed in previous literature [24] as the effects on larger scale behavior are secondary. A structured mesh was used to better capture the sharp front that is created, with four divisions used in the vertical direction as the problem is essentially one-dimensional. This is because the small thickness of the paper relative to its length means that vertical equilibrium occurs so quickly that a one-dimensional simulation would have also been appropriate. A two-dimensional domain was however investigated to make the initial surface saturation boundary condition where the droplet resides more intuitive. The results of a mesh refinement study are shown in supplementary information for an n value of 8. This value was chosen as it is higher than any n value used in results and therefore represents a worst case, where the simulation would be most dependent on mesh quality. This is because higher n values cause a sharper interface to form. A mesh spacing of $\delta x = 0.02R_0$ was chosen as this kept simulations to a reasonable time and corresponded to less than a 5% variation from the finest mesh tested. To simulate the first stage a time step $\delta t = 0.01$ s was chosen to ensure that t_{abs} was calculated to sufficient accuracy. During the second stage the time step was increased incrementally to a maximum of 0.04 s to save computational time. Time step sensitivity analysis of the same test case as the mesh resolution study was carried out, showing that the choice of $\delta t =$ 0.01–0.04 s was sufficient for accuracy and stability of the numerical solution.

Stain boundary was calculated by identifying a radial position that corresponded to a relative volume fraction (ϕ) of 0.01. As volume fraction decreases extremely quickly near the edge of a stain, the criterion of stain front definition did not affect results. This model uses 7 input parameters: V_D droplet volume, μ viscosity, h paper thickness, D_0 diffusivity at maximum saturation, n linear function of pore distribution index, A_0 initial droplet area and ϵ_s saturation volume fraction. While some of these parameters can be directly measured and some must be fitted, all have a physical meaning in the first stage of the simulation. As n is only based on pore distribution index in the first stage it is an empirical fitting parameter in the second.

2.2. Experimental

2.2.1. Materials

Analytical grade glycerol, decane and ethanol were purchased from Merck, Sigma and Thermo Fisher Scientific, respectively. Densities of glycerol, decane and ethanol solutions were interpolated from data measured by Sheely [25], Liu et al. [26] and Khattab et al. [27] respectively. Tests were performed on Whatman 41 filter paper and Advantec GA-55 glass fiber filters. Deionized water for tests and dilutions was purified from tap water with a Direct-Q water purification system to a minimum resistivity of 18.2 MΩ·cm. Queens blue food dye was used to dye water soluble fluids.

2.2.2. Methods

Droplets were produced with an adjustable needle and a syringe pump in the same way as our previous study [14]. The syringe pump provided a constant flow rate to the needle which causes droplets of repeatable size to detach and periodically fall from the needle. Droplet size was quantified using a Mettler Toledo TLE balance before the needle was directed onto the paper surface. The average weight of 4 previous droplets divided by the density of the fluid was used to estimate the volume of the droplet that fell onto the paper. Droplet size was controlled by altering needle size. Stain size data were recorded by a Point Grey Flea3 camera mounted on a track that captured the reflected bottom view of the paper. The images were captured at 120 frames per second. A diagram of the experimental setup is shown in Fig. 2. All tests were performed in a 23 °C 50% relative humidity environment. To

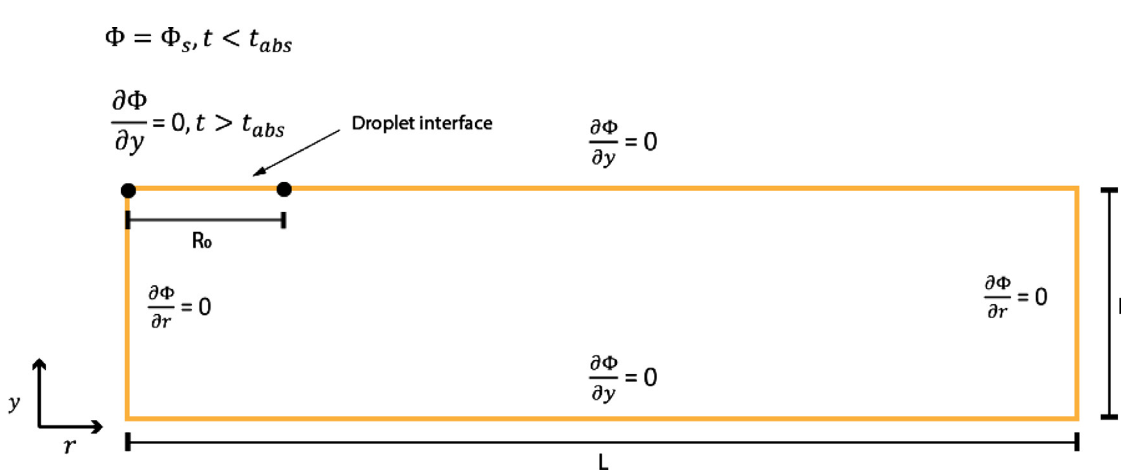

Fig. 1. Diagram of simulation domain with implemented boundary conditions.

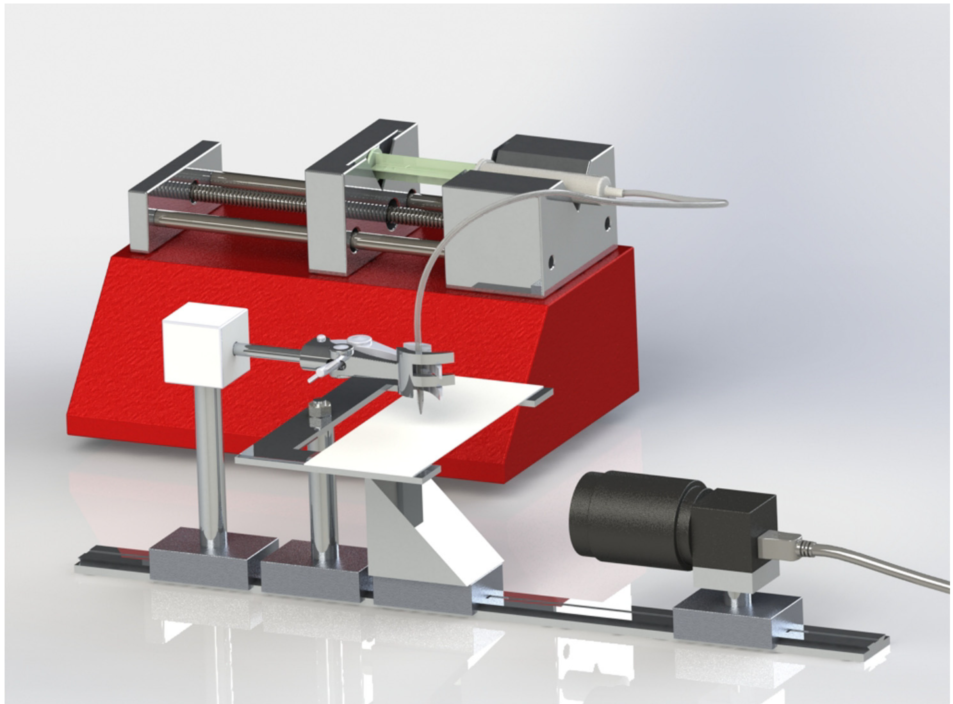

Fig. 2. Syringe pump and needle experimental setup. The side mounted camera and 45 degree mirror are shown.

improve contrast, 3 wt% of food dye solution was added to the aqueous solutions. Tests were performed to ensure the dye at the concentration studied did not affect results. Although the dynamic wicking measurements without dye were prone to noise, there was no significant differences between dyed and not dyed fluids. This dye was assumed to have the same properties as water and was included in solution concentration calculations. Droplet disappearance times were found using a side mounted Phantom VEO 410L high speed camera recording at 4000 fps. No adequate dye was found for decane as all dyes separated chromatographically due to their affinity for cellulose. Due to this, no contrast agent was used and as a result there is more noise in the decane recordings.

2.2.3. Porosimetry

Porosimetry measurements were performed with a mercury porosimeter (Micrometrics AutoPore IV 9500). This characterises the infiltration against pressure. To convert this into data that can be compared to Eq. (7), the infiltration values were divided by their maximum value; this gave infiltration data relative to maximum saturation. The pressures were converted to a radius and then back to a pressure using the Laplace equation applied on circular capillaries using the surface tension of mercury and then back with the surface tension of water. The values of surface tension and contact angle used are shown in Table 1.

3. Results

3.1. Porosimetry

To verify the use of Eq. (6), porosimetry measurements were carried out. This allowed the fitting of model pressure curves (Eq. (7)) to porosimetry data to determine the pore distribution index and therefore the value of n. Fig. 3 shows the comparison between porosimetry data calculated using the surface tension and contact angle of water. A pressure curve corresponding to an n value of 2.2 is fitted, with good correlation between model and experimental data.

3.2. Initial penetration

Simultaneously recording the side and bottom views of the paper substrate allowed the delay between droplet impact and stain appearance to be measured on all types of paper tested. A high-speed recording of this imaged at 8000 fps is given in supplementary information. This recording shows that the vertical

Table 1
Fluid properties used.

Fluid	Concentration wt%	Density (kg/m^3 × 10^3)	Surface Tension (mN/m)	Viscosity (mPa·s)	Advancing contact angle on cellulose (deg)
Mercury	100%		485 [28]		130 [28]
Water	100%	1.00 [29]	72.31 [30]	0.93 [29]	13.5 [14]
Glycerol	10%	1.02 [25]	71.97 [31]	1.21 [25]	
Glycerol	20%	1.05 [25]	71.4 [31]	1.63 [25]	
Glycerol	40%	1.10 [25]	69.6 [31]	3.40 [25]	
Glycerol	60%	1.15 [25]	68.1 [31]	9.63 [25]	
Ethanol	20%	0.93 [27]	32.27 [27]	2.52 [27]	
Ethanol	40%	0.89 [27]	27.65 [27]	2.49 [27]	
Ethanol	90%	0.80 [27]	23.09 [27]	1.38 [27]	
Decane	100%	0.73 [26]	24.47 [26]	0.85 [26]	

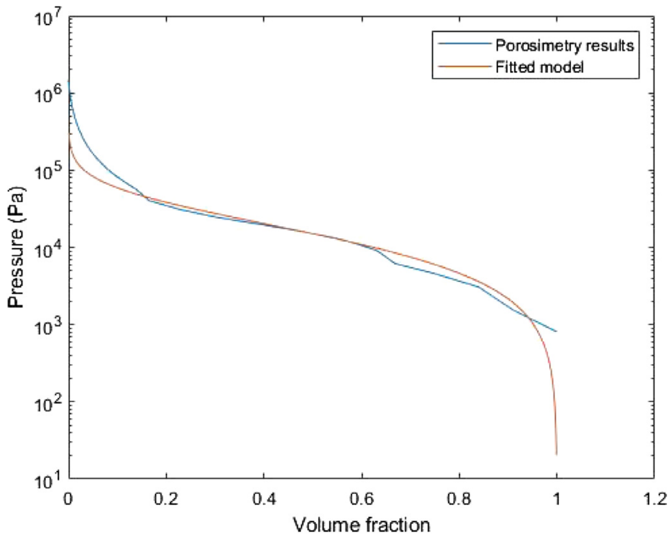

Fig. 3. Comparison of the theoretical model (Eq. (7)) with the mercury porosimetry measurement on Whatman 41 filter paper. Volume fraction is calculated as the volume of fluid in the paper divided by the volume at maximum saturation.

penetration of the droplet into paper occurs so quickly as to be considered instantaneous over the time scale of the stain growth. This finding was consistent for all types of paper tested. This very short time scale of vertical penetration also shows that the vertical variation of fluid will be insignificant in this study. This, combined with ignoring the variation between the paper machine (MD) and cross (CD) directions that is known to cause slightly elliptical stains [32] allows the process to be considered as one dimensional.

3.3. Stain growth

The stain sizes with time for a series of model fluids on Whatman 41 paper are shown in Fig. 4. The stain size data was recorded over different time intervals. The main focus was on the early to mid stages and longer recordings took up significant hard disk space and were minimised. Due to this, the relative length of the curves in Fig. 4 vary and are only indicative of the recording time. The wicking behaviour of droplets of water, ethanol and glycerol solutions on paper was studied. These liquids were selected to provide a variety of viscosity and surface tension conditions for a homologous series of fluids. Droplets of different diameter were deposited on paper and the stain area was recorded as a function of time. Results show that the larger droplets cause larger stain area; however, these area kinetics measurements are not scalable by any simple function of droplet volume. In some cases, droplets of slightly larger volumes created smaller stain sizes or vice versa (Fig. 4d); the droplet volume difference over which this occurs gives an indication of experimental error. Fluids of high surface tension wick faster than fluids of low surface tension. Fluids of high viscosity wick slower than fluids of low viscosity. These trends are consistent with Marmur's equation [12] (Eq. 2) as well as the Lucas-Washburn equation [6].

3.4. Transition point

A two-stage wicking behavior becomes clearly apparent on a log-log scale for all fluids tested. The linear counterparts to the data in Fig. 4 are shown in supplementary information. The transition point between the two stages was identified from the sudden change in the gradient in the log-log curves. The questions to address are therefore whether these two stages have a physical meaning, and what are the mechanisms driving the phenomena.

From the gradient of the log-log curves, the exponent m (Eq. (1)) can be calculated before and after transition. For all aqueous solutions tested on paper, the value of m for each system ranged between 0.26–0.44 for the first stage and between 0.12–0.20 for the second stage. These values are slightly lower than those reported in most previous studies on radial wicking [1,2,10].

Fig. 5 shows the results of the same test with decane. In this case there is no clearly defined transition point, and the stains are much larger than those from similar volumes of aqueous solutions at all times. This size difference is highlighted by the plot utilising the same axis dimensions as those in Fig. 4.

Before stain growth data for different fluids can be compared (Fig. 4), several droplets of similar size but from different fluids must be compared. Unfortunately, due to varying densities and surface tensions of fluids, any needle of a given diameter produced droplets of different size for different fluids. This meant it was not always possible to accurately predict the size of the droplet. Reproducing identically sized droplets proved challenging for the different fluids. To overcome this issue, the data was fitted to a function of volume at every frame to determine the area's dependence on droplet volume at that time. This function could then be interpolated to a desired droplet volume to estimate the stain area at any volume for each frame. By combining these interpolated area values, an estimate of the spreading dynamics could be calculated. The results from interpolation agree with experimental data extremely well and all areas were found to be strongly linear with droplet volume at any given time. This means that the dynamics of stain growth of a droplet of any size can be predicted accurately using the results of two droplet sizes. This linearity was also demonstrated in our previous study [14], where the area to droplet volume relationship at equilibrium was found to be linear.

Using the data in Fig. 4, the area of the stain at the transition can be plotted as a function of droplet volume. This is shown in Fig. 6a. This demonstrates that the stain transition area forms a linear relation with droplet volume and is independent of fluid properties. Aqueous solutions at high concentrations of ethanol and glycerol deviate from this trend slightly.

Fig. 6b illustrates the timing of the stain transition point relative to the timing of droplet disappearance above the surface of the paper for water, 40% ethanol and 60% glycerol solutions. The same figure with data from all water solutions is in supplementary information. Fig. 6b also shows that linear fits are reasonable for both stain size transition and droplet disappearance. Using these linear fits for all fluids, the timing of stain size transition and droplet disappearance of a 10 μL droplet is interpolated and compared in Fig. 6c. It shows that the timing of the two phenomena is related; as one gets longer, the timing of the other generally follows proportionally. The figure also shows that droplet disappearance always occurs before the stain growth transition.

4. Discussion

4.1. Stain growth

Fig. 7 shows the results of an interpolation for the wetting area produced by a 10 μL droplet of several model fluids on Whatman 41 filter paper for the beginning of the wicking period. There are minor differences in the transient behavior of the stain area kinetics among the various aqueous solution droplets. However, the late stages appear to converge. This late stage convergence was discussed in our previous study [14] where the equilibrium stain size was analysed for a series of fluids. Here, decane produces a much larger stain size than those from the other fluids tested, despite having a similar surface tension to the 90% ethanol solution. The viscosity of decane is slightly lower than that of any other fluids

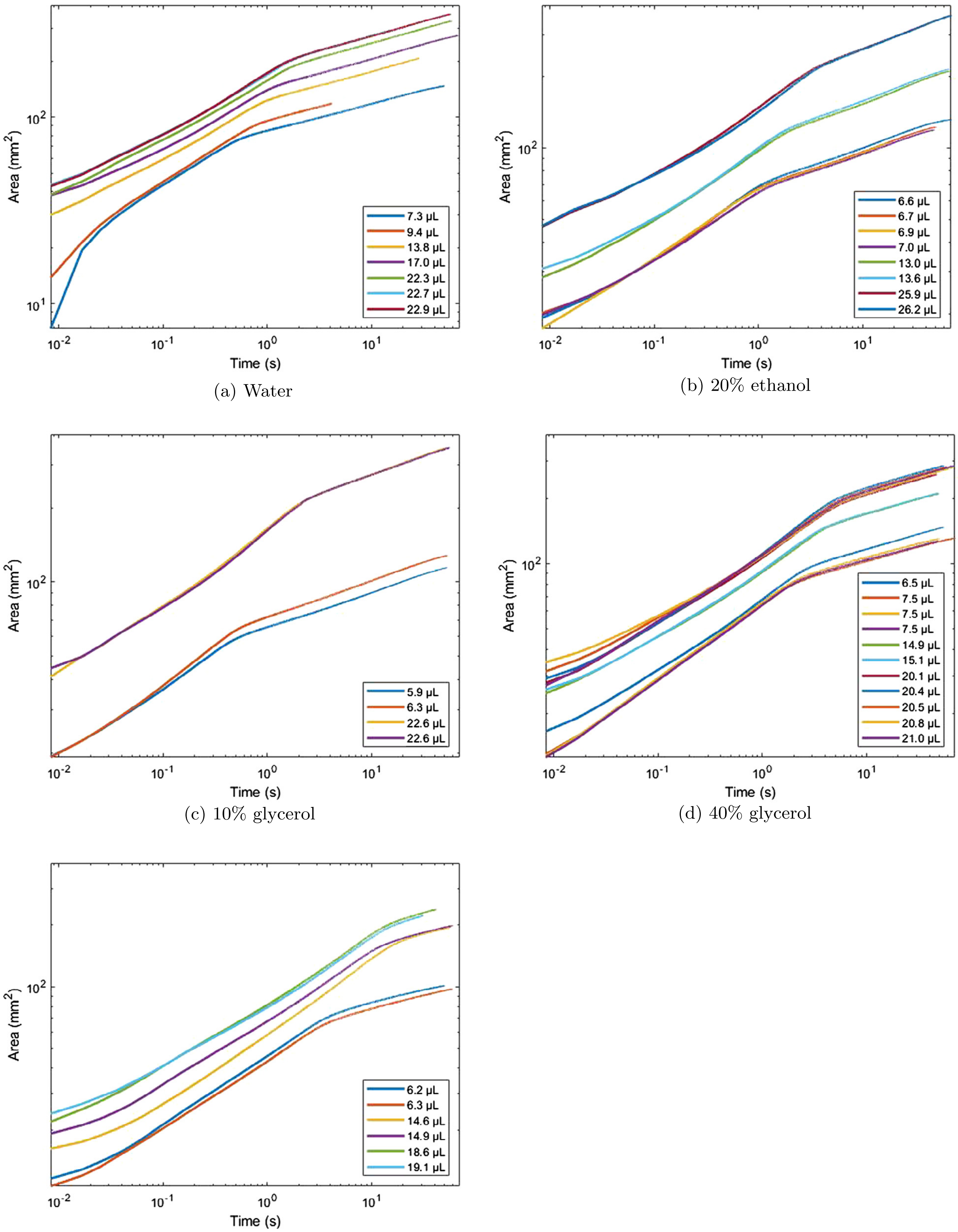

(a) Water

(b) 20% ethanol

(c) 10% glycerol

(d) 40% glycerol

(e) 60% glycerol

Fig. 4. Evolution of stain size with time for a variety of fluids and droplet sizes on Whatman 41 filter paper.

studied (Table 1). However, based on the relatively low sensitivity to viscosity found with the other measurements, it is unlikely that the slightly lower viscosity of decane is responsible for the huge discrepancy in stain behaviour observed. The high stain size of decane was previously attributed to the purely non-polar behaviour of the fluid, preventing any swelling of the cellulose fibers through relaxation of the intra and inter hydrogen bonding among fibers [3]. Swelling of fibers results in a smaller amount of fluid

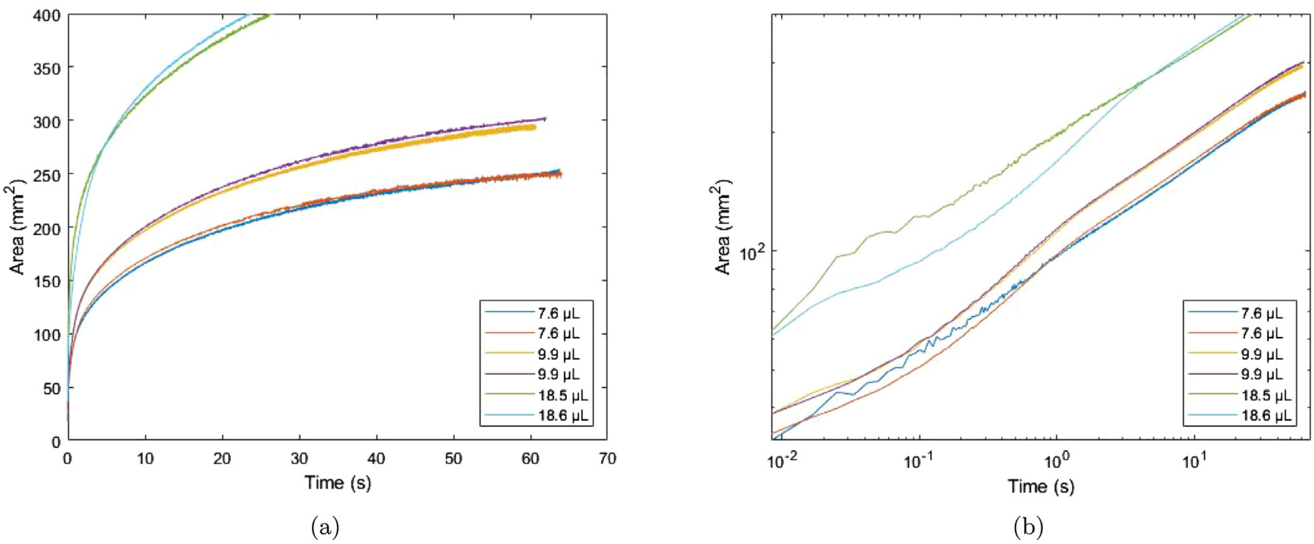

Fig. 5. Stain size with time for decane on filter paper.

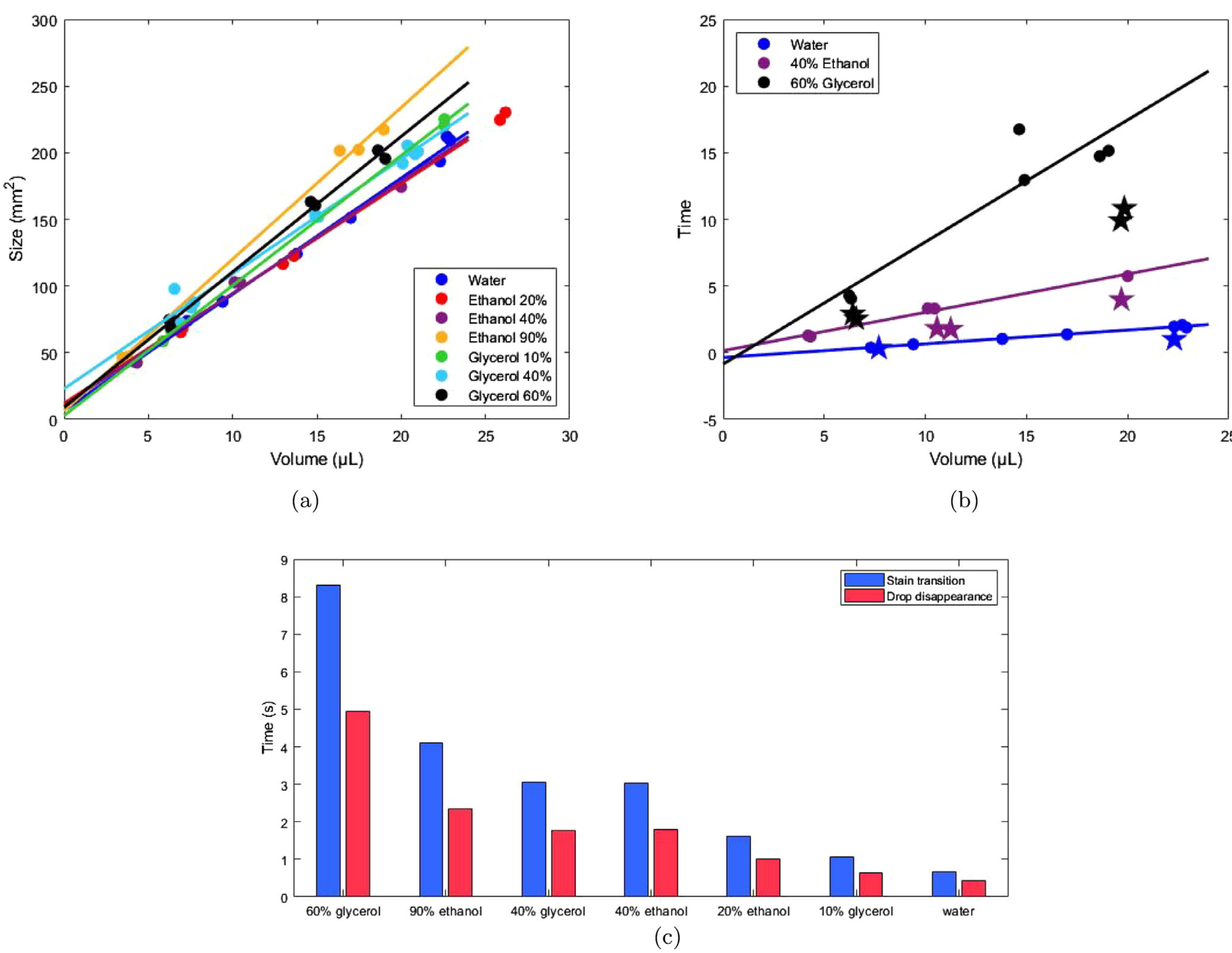

Fig. 6. (a) Area at which stain transition occurs with droplet volume for all model fluids. (b) Time at which the stain wicking transition occurs as a function of droplet volume for 3 representative fluids. Stars represent the time at which each droplet disappears from the surface of paper. (c) Interpolated stain size transition and drop disappearance time data at 10 μL.

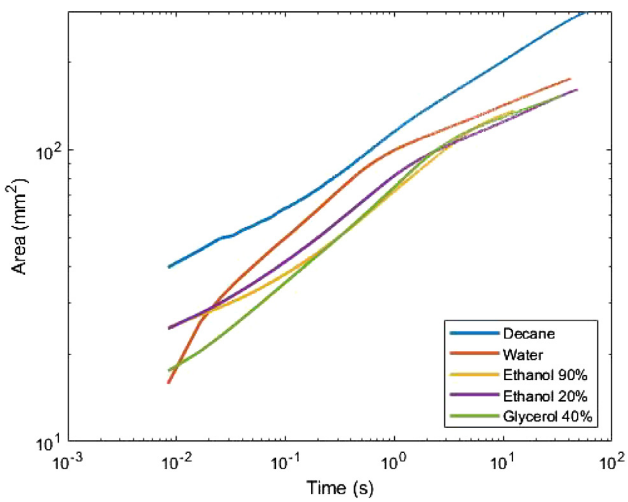

Fig. 7. Interpolated data showing the spreading of 10 μL droplets on a loglog scale.

available, therefore effectively decreasing the liquid volume available to wick out. The swelling fibers will also physically become larger, decreasing pore size [33]. Neither the effect of pore size change or liquid consumption has been thoroughly quantified. Schuchard and Berg [33] studied the effect of swelling fibers on vertical imbibition from an infinite reservoir. They reported the difference between a swelling and a non-swelling fluid could be accounted for by a reduction of the effective capillary radius in the Lucas-Washburn equation [5,6] for normal paper fibers.

4.2. Mechanism of the stage transition

A two-stage wicking regime is clearly seen on the log-log scale of stain size as a function of time (Fig. 4). These regimes are very reproducible and were systematically observed for all fluids except for decane on paper. Several explanations for this two-stage process were investigated. First, as decane is known not to swell cellulose fibers [33] the transition could indicate the time at which the fibers have swollen by an amount that would affect wicking. Tests on filter papers performed with glass fibers (non-swelling) are given in supplementary information and also revealed a two-stage process, very similar to that observed on cellulosic fibers. This observation reveals that swelling is unlikely to be responsible. A second possible explanation is the absorption of the droplet into the paper. This process is likely to affect results as its timing correlates with the stain transition (Fig. 6b). However, as this absorption also occurs with decane droplets, it is unlikely to be a dominant mechanism. Third, the transition could represent a transition from wicking through a fully saturated to a partially saturated substrate. This is likely to affect results; however, as there is little previous work on the subject, the dominance of this mechanism is unknown and needs to be further probed. This was achieved here by modelling.

The transition from a fully saturated to a semi saturated mechanism also explains the delay seen between stain transition and droplet disappearance shown in Fig. 6b. It is reasonable to assume that the propagation of the effect of the droplet disappearance (lowering of the local volume fraction), requires a finite period of time to reach the outside of the stain. Also, the decreased volatility of decane, compared to aqueous solutions, is unlikely to be responsible for the change in transition phenomena as it would result in a smaller amount of evaporation occurring. Our previous study demonstrated [14] that even with the more volatile fluids, no significant evaporation occurs over the time scale studied. Therefore, lowering the evaporation further is expected to have no effect.

4.3. Simulation results

The model developed predicts the wicking behavior of sessile droplets onto a porous surface. It requires 7 input parameters to calculate stain size as a function of time: droplet volume (V_D), viscosity (μ), paper thickness (h), scaled diffusivity at saturation (D_0), pore distribution index (λ), initial wet area (A_0) and saturation volume fraction (ϵ_s). Each of these variables has a clear physical meaning and most can be identified experimentally [16]. Although the choice for droplet volume, paper thickness and viscosity is trivial, the selection of the remaining variables is more difficult. For the given case, a value for n and therefore λ was extrapolated from porosimetry measurement in Fig. 3, and a value for A_0 was found by scaling the stage one data with Marmur's equation (Eq. (2)). The value of A_0 that results in a linear relation with time is chosen as the A_0 for that situation. An estimation for ϵ_s can be found by measuring the difference between the dry weight and the wet weight of a paper sample. This was reported for Whatman 41 filter paper previously [14] and the volume fraction of water in wet paper can be calculated to be 0.62. The testing standard used (TAPPI 441) for wet weight characterisation includes a rolling step between blotting papers that is designed to remove excess water. However, this rolling method might also remove some excess water that will otherwise remain in a droplet wicking case. For these reasons, the actual saturated value is likely to be slightly higher than measured. A value of $\epsilon_s = 0.7$ best fits our results. The results of a simulation with these calculated parameters and fitting just the D_0 value is shown in Fig. 8. Parameter used in this simulation are shown in Table 2. Viscosity of water is taken from literature [29].

Although modelling well represents experiments in the first stage, poor agreement is observed for the second stage. It is clear that the 7 parameters chosen do not fit the second stage. This is not surprising, as only infusion porosimetry data was used to calculate n. Hysteresis in porosimetry experiments is well documented [34] and its relevance to wicking reported [35]. As the liquid redistribution (second) phase is dominated by the emptying of pores, it is not surprising that a single value of n cannot capture both the first and second stages. Fig. 9 shows the results of a simulation with a value of n that changes for the second stage. This value was found by fitting the stain area data. This value could not be externally calculated because it is an effective n for the specific combination of infiltration and redistribution occurring in the second stage which is rather complex. Both experimental

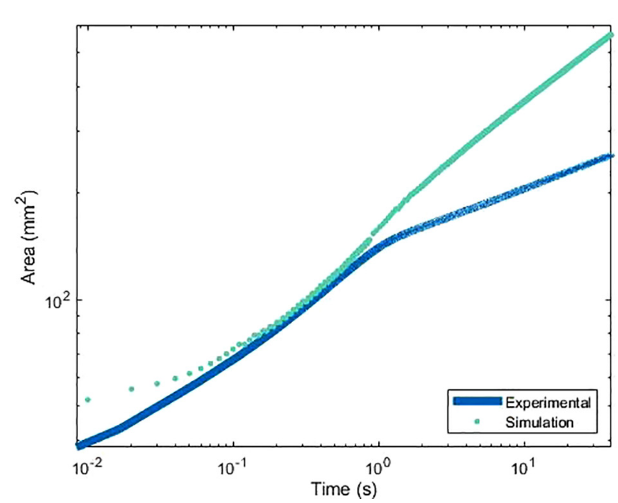

Fig. 8. Comparison of experimental versus calculated values of area as a function of time on a log-log scale.

Table 2
Parameters used for Fig. 8.

Parameter	Value
V_D	17 μL
μ	0.93 mPa·s
h	226 μm
D_0	12.09 nPa·m^2
A_0	43.01 mm^2
ϵ_s	0.7
n	2.2

Table 3
Parameters used for Fig. 9.

Parameter	Water Case	40% Glycerol Case
V_D	17 μl	17 μL
μ	0.93 mPa·s	3.40 mPa·s
h	226 μm	226 μm
D_0	12.09 nPa·m^2	12.09 nPa·m^2
A_0	43.01 mm^2	43.01 mm^2
ϵ_s	0.7	0.7
n stage 1	2.2	2.2
n stage 2	5	4

and simulation results are also shown for a 17 μL droplet of water and 40% glycerol solution in Fig. 9. The only difference between these two simulations is a change in the viscosity parameter and a refitted second stage n value. Parameters used are given in Table 3. The viscosity of a 40% glycerol solution was interpolated from results of Sheely [25]. The fitted value for second stage n was different between the two fluids, with each requiring a different fitted n value for the second stage. The fitted value for n during the second stage is 5 and 4 for water and glycerol respectively. The experimental results for glycerol are interpolated from data in Fig. 4d as a droplet of exactly 17 μL droplet was not tested. The water case is very well described by the model except for a slight deviation at later times. This is most likely because evaporation and swelling become more dominant in the later stages and are not included in this model. The glycerol simulation predicts behavior very well in the first stage; however, it deviates more than water in the second. This implies that higher viscosities slightly invalidate the assumption that the redistribution of fluid can be represented by a simple constant exponent n. Although the broad behavior is still represented. Simulations of different droplet sizes with appropriate changes to V_D and A_0 and keeping all else constant also fit experimental data. However, small droplets (<10 μL) are not well described by the model. This is likely because the small reservoir results in a larger fraction of the stain having never achieved full saturation. This would make redistribution more dominant through the whole process, and would mean that both the calculated n value for the first stage and the fitted value of n for larger droplets for the second stage may not be an appropriate choice. The constant size of the fully saturated boundary condition in the first stage would also be less appropriate for a small droplet [24].

The abrupt transition from stage one to stage two and the flat region immediately after is caused by the sudden shift in n at the stage transition of the simulation. In reality, both the transition from saturated to a no flux boundary condition and the change in n value happens gradually as the droplet is consumed and the dominant spreading mechanism changes from infiltration to redistribution. This is a simplification and a more complete model would account for this gradual shift. Not enough is known about porosimetry hysteresis and how it is affected by local volume fraction history to account for this effect. However, the broad effects are well described by the simplification introduced here. It is also relevant that the simulation results for the no hysteresis case (Fig. 8) look very similar to results with decane in that no significant transition is observable. The simulation can be made to fit decane results with a single value of n, however this requires new fitted values for A_0, D_0 and n. This may be because the wetting characteristics of decane on cellulose are such that the diffusivity experiences no significant hysteresis, and this affects the calculated parameters.

Although surface tension and contact angle of the fluid are used in calculating n from porosimetry data, these are also likely to effect A_0 and D_0; these were not included as input parameters in the model. Both of these quantities for water and glycerol are very similar [31], which explains why the model still fits experimental data between these two fluids.

The results of these simulations show that there are two dominant driving mechanisms behind the two-stage transition. First, the change from saturated to non-saturated boundary conditions at the center of the stain. Second, a change in how pressure and permeability vary as functions of volume fraction between systems that are dominated by pore filling and pore emptying.

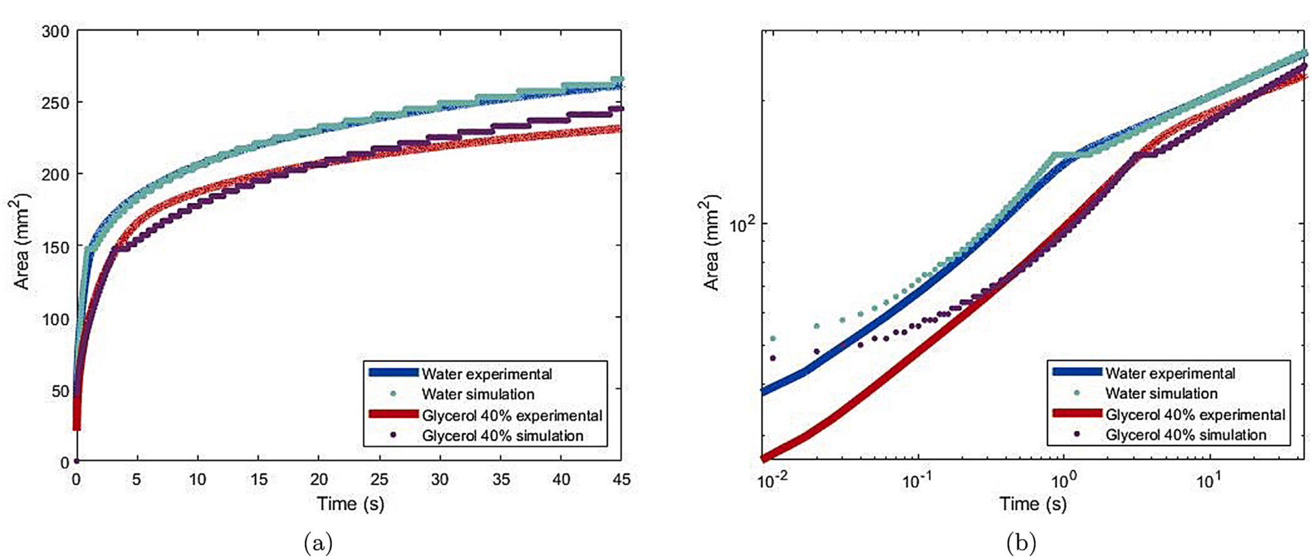

Fig. 9. Simulation and experimental results for water and 40% glycerol solution on a linear and log-log scale.

5. Conclusion

The evolution in time of the stain area produced by a sessile droplet deposited on paper was measured, modelled and analysed. A series of fluids varying in surface tension and viscosity was examined. A new model to describe the data has been developed based on Richards' equation [21] and is easily resolved numerically in one dimension using experimentally measured boundary conditions and input parameters. This expands on previous work [10–12,15,18] where imbibition into linear and radial systems from an infinite reservoir has been investigated and modeled.

Radial wicking kinetics with all tested liquids besides decane showed two-stages, with a fast initial growth regime followed by a slower regime. The first regime corresponds to the liquid absorbing into the paper by wicking, while the second represents liquid redistribution [2]. This work identifies the cause of the transition between the two regimes to be the disappearance of the droplet coupled with the shift in mechanism due to the redistribution occurring in the second phase. This modeling technique also describes well the experimental results for both regimes. Further, the 7 parameters of the model have all a physical meaning and can be either measured experimentally or calculated.

This research contributes to the fundamental understanding of the wicking mechanism. The proposed modeling technique allows the quantification and prediction of stain dynamics in a variety of industrially relevant situations that were previously deemed too complex. The wicking of a finite reservoir is a common process in the printing, textile, agriculture and medical industries, and the development of a method of prediction will assist in the design and optimisation of new technologies. This study also provides a rigorous and physically meaningful alternative to the semi-empirical Lucas-Washburn equation to describe the wicking kinetics of droplets in real porous media.

Acknowledgments

This research was funded by an ARC Linkage grant (LP160100544) and Haemokinesis.

Appendix A. Supplementary material

Supplementary data associated with this article can be found, in the online version, at https://doi.org/10.1016/j.jcis.2019.01.032.

References

[1] E. Kissa, Capillary sorption in fibrous assemblies, J. Colloid Interface Sci. 83 (1) (1981) 265–272.
[2] D. Danino, A. Marmur, Radial capillary penetration into paper: limited and unlimited liquid reservoirs, J. Colloid Interface Sci. 166 (1) (1994) 245–250.
[3] T. Kawase, S. Sekoguchi, T. Fujii, M. Minagawa, Capillary spreading of liquids, Text. Res. J. 56 (7) (1986) 409–414.
[4] K. Borhan, A. Rungta, An experimental study of the radial penetration of liquids in thin porous substrates, J. Colloid Interface Sci. (1993) 403–411.
[5] V.R. Lucas, Ueber das zitgesetz des kapillaren aufstiegs von flüssigkeiten, Kolloid-Zeitschrift 23 (1) (1918) 15–22.
[6] E.W. Washburn, The dynamics of capillary flow, Phys. Rev. 17 (3) (1921) 273–283.
[7] K. Li, D. Zhang, H. Bian, C. Meng, Y. Yang, Criteria for applying the lucas-washburn law, Sci. Rep. 5 (2015) 1–7.
[8] M.M. Gong, D. Sinton, Turning the page: Advancing paper-based microfluidics for broad diagnostic application, Chem. Rev. 117 (12) (2017) 8447–8480.
[9] E. Elizalde, R. Urteaga, C.L.A. Berli, Rational design of capillary-driven flows for paper-based microfluidics, Lab Chip 15 (10) (2015) 2173–2180.
[10] T. Gillespie, The spreading of low vapor pressure liquids in paper, J. Colloid Sci. 13 (1) (1958) 32–50.
[11] A. Borhan, K.K. Rungta, On the radial spreading of liquids in thin porous substrates, J. Colloid Interface Sci. 154 (1) (1992) 295–297.
[12] A. Marmur, The radial capillary, J. Colloid Interface Sci. 124 (1) (1988) 250–256.
[13] A. Marmur, Penetration and displacement in capillary systems of limited size, Adv. Colloid Interface Sci. 39 (C) (1992) 13–33.
[14] M.J. Hertaeg, R.F. Tabor, G. Garnier, Effect of protein adsorption on the radial wicking of blood droplets in paper, J. Colloid Interface Sci. 528 (2018) 116–123.
[15] A. Perez-Cruz, I. Stiharu, A. Dominguez-Gonzalez, Two-dimensional model of imbibition into paper-based networks using Richards' equation, Microfluid. Nanofluid. 21 (5) (2017) 1–12.
[16] D. Rath, N. Sathishkumar, B.J. Toley, Experimental measurement of parameters governing flow rates and partial saturation in paper-based microfluidic devices, Langmuir 34 (30) (2018) 8758–8766.
[17] S. Jaganathan, H.V. Tafreshi, B. Pourdeyhimi, A realistic modeling of fluid infiltration in thin fibrous sheets, J. Appl. Phys. 105 (11) (2009), https://doi.org/10.1063/1.3141737.
[18] A. Ashari, T.M. Bucher, H.V. Tafreshi, M.A. Tahir, M.S. Rahman, Modeling fluid spread in thin fibrous sheets: Effects of fiber orientation, Int. J. Heat Mass Transf. 53 (9-10) (2010) 1750–1758.
[19] S.C. Chapra, R.P. Canale, Numerical Methods For Engineers, Mcgraw-Hill, New York, 1998.
[20] W.L. Then, M. Li, H. McLiesh, W. Shen, G. Garnier, The detection of blood group phenotypes using paper diagnostics, Vox Sang. 108 (2) (2015) 186–196.
[21] L.A. Richards, Capillary conduction of liquids through porous mediums, J. Appl. Phys. 1 (5) (1931) 318–333.
[22] H. Huinink, Fluids in Porous Media, Morgan & Claypool Publishers, 2016.
[23] D.J.E. Harvie, An implicit finite volume method for arbitrary transport equations, ANZIAM J. 52 (0) (2012) 1126–1145.
[24] V.M. Starov, S.A. Zhdanov, S.R. Kosvintsev, V.D. Sobolev, M.G. Velardec, Spreading of liquid drops over porous substrates, Adv. Colloid Interface Sci. 104 (2003) 123–158.
[25] M.L. Sheely, Glycerol viscosity tables, Ind. Eng. Chem. 24 (9) (2013) 1060–1064.
[26] Y. Liu, R. Difoggio, K. Sanderlin, L. Perez, J. Zhao, SMeasurement of density and viscosity of dodecane and decane with a piezoelectric tuning fork over 298-448 K and 0.1-137.9 MPa, Sens. Actuators, A 167 (2) (2011) 347–353.
[27] I.S. Khattab, F. Bandarkar, M.A.A. Fakhree, A. Jouyban, Density, viscosity, and surface tension of water+ ethanol mixtures from 293 to 323 K, Korean J. Chem. Eng. 29 (6) (2012) 812–817.
[28] H. Giesche, Mercury porosimetry: A general (practical) overview, Part. Part. Syst. Char. 23 (1) (2006) 9–19.
[29] J. Kestin, M. Sokolov, W.A. Wakeham, Viscosity of liquid water in the range- 8 C to 150 C, J. Phys. Chem. Ref. Data 7 (3) (1978) 941–948.
[30] G. Vazquez, E. Alvarez, J.M. Navaza, Surface tension of alcohol water+ water from 20 to 50. degree. C, J. Chem. Eng. Data 40 (3) (1995) 611–614.
[31] K. Takamura, H. Fischer, N.R. Morrow, Physical properties of aqueous glycerol solutions, J. Petrol. Sci. Eng. 98 (2012) 50–60.
[32] N. Walji, B.D. MacDonald, Influence of geometry and surrounding conditions on fluid flow in paper based devices, Micromachines 7 (5) (2016) 73.
[33] D.R. Schuchard, J.C. Berg, Liquid transport in composite cellulose-superabsorbent fiber networks, Wood Fiber Sci. 23 (3) (2007) 342–357.
[34] J. Kloubek, Hysteresis in porosimetry, Powder Technol. 29 (1) (1981) 63–73.
[35] M. Landeryou, I. Eames, A. Cottenden, Infiltration into inclined fibrous sheets, J. Fluid Mech. 529 (2005) 173–193.